Bull. Mater. Sci. (2020) 43:64
https://doi.org/10.1007/s12034-020-2045-4

Monovalent (Li^{+1}) doping effect in multiferroic $GdMnO_3$

RINKU SARKAR, BIDYUT SARKAR and SUDIPTA PAL*
Department of Physics, University of Kalyani, Kalyani, Nadia 741235, India
*Author for correspondence (sudipta1@klyuniv.ac.in)

MS received 16 August 2019; accepted 6 December 2019

Abstract. This paper reports the temperature- and field-dependent magnetic properties of monovalent-doped polycrystalline sample $Gd_{0.85}Li_{0.15}MnO_3$ (GLMO) prepared by conventional solid-state reaction route. Final sintering at 1673 K for 18 h yields in the formation of well-grown, impurity phase free, single-phased, orthorhombic structured (with *Pbnm* space group) crystal. The optical properties have been investigated by UV-absorption spectra. The room temperature UV-absorption spectrum using Tauc's formula gives an optical band gap of ~3.12 eV. The paramagnetic (PM) state to incommensurate antiferromagnetic (ICAFM) state transition temperature increases due to Li doping. Magnetic hysteresis curve at 5 K signifies the Gd spin ordering.

Keywords. Manganites; optical properties; magnetic properties; magnetic phase transition.

1. Introduction

In recent years, multiferroic-based manganites ($RMnO_3$ with R = Tb, Dy, Gd) have attracted much attention. They are superlative materials for the study of the magneto-electric effect, because of strongly competing magnetic interactions [1–5]. In orthorhombic $RMnO_3$ with perovskite structure, the ferroelectricity appears because of a complex spiral spin order that breaks the inversion symmetry [6,7] and magnetic transition takes place at much lower temperatures [8]. $GdMnO_3$ (GMO) is an interesting multiferroic material. The ionic radius of Gd lies in between La and Dy in the rare earth family, for this, its physical properties is a sensitive function of strain. In GMO, the interaction between Gd 4f spins and Mn 3d spins generates various magnetic transitions at different temperatures [5]. Mn^{3+} spins are ordered to an incommensurate state below T_N ~43 K and into a canted antiferromagnetic state between 16 and 23 K with small ferromagnetic ordering due to the polarization of Gd 4f spins. Below 6.5 K due to the interaction of 4f spins, long-range ordering of Gd moment occurs. At this temperature, canted Gd moments completely ordered opposite to the ferromagnetic canted Mn moments [8,9]. The crystal structure in GMO is described by *Pbnm* space group with an orthorhombic perovskite structure at room temperature [8,10,11]. The magnetic properties of undoped and divalent/trivalent-doped GMO have been studied by several researchers. Biswas *et al* [12] and Snyder *et al* [13] observed that $Gd_{1-x}Ca_xMnO_3$ ($x = 0.30, 0.33$) shows ferrimagnetic nature and at low temperature, in the presence of low magnetic field, they show magnetization reversal. This kind of magnetic properties also observed in $Pr_{1-x}Gd_xMnO_3$ [14]. But the effect of monovalent cation doping at Gd site is also interesting. Here, we have studied the effect of monovalent Li doping at Gd site on the magnetic properties of $GdMnO_3$ compounds. Fifteen mole percent Li doping converts 30 mol% Mn^{3+} to Mn^{4+} due to which $Gd_{0.85}Li_{0.15}MnO_3$ compound show paramagnetic to antiferromagnetic phase transition with Neel temperature ~42 K.

2. Experimental

Hole-doped polycrystalline sample $Gd_{0.85}Li_{0.15}MnO_3$ (GLMO) was synthesized in the air by conventional solid-state reaction method. Gadolinium oxide (Gd_2O_3), manganese oxide (MnO_2), lithium nitrate ($LiNO_3$) were taken as raw materials. At first, they were preheated at 573 K for 2 h to avoid the moisture and then mixed with their stoichiometric ratios in a mortar and grounded for 2 h with a little addition of propan-2-Ol alcohol. The powder was initially calcined at 873 K for 9 h, then, cooled down to normal temperature. This preheated powder was reground and pressed into cylindrical pellets, calcined at 1173 K for 12 h, and cooled down. Then, the final pellets were sintered at 1673 K for 18 h. Then, the sample was furnace cooled with natural cooling rate and collected for further measurements.

Structural characterization of the sample was examined by using powder X-ray diffraction (XRD). The phase purity was checked by analysing the XRD data using FULLPROOF suit software with the help of pseudo-Voigt profile (or pseudo-Voigt function). The UV–visible spectrum was recorded with UV-3600 spectrometer. All magnetic measurements were performed by using SQUID magnetometer, whose temperature range is 2–330 K. Magnetization (M) *vs.* temperature (T) measurements in various field (H) conditions were recorded

Published online: 10 February 2020

in the temperature range of 5–300 K in both zero field cooled (ZFC) and field cooled (FC) modes in the presence of various applied external magnetic fields. In ZFC mode, sample was cooled down to 5 K in zero fields and then, an external field was applied to collect the data of the in-heating cycle. Again, in FC mode, the sample was cooled down to 5 K with the help of preferred field, and data was recorded in the heating cycle in the presence of the same applied field. Magnetization–field (M–H) data were measured in SQUID magnetometer within the field values ranging from −50 to 50 kOe at 5 K.

3. Results and discussion

The powder XRD profile of GLMO manganite is shown in figure 1. The well-fitted Rietveld refinement of the XRD data using the FULLPROF program assures that the sample possesses single phase orthorhombic perovskite structure and the crystal structure belongs to *Pbnm* space group. The refined lattice parameters, atomic positions, discrepancy factors are stated in table 1. References [10,11] also confirm that the sample is a member of the orthorhombic crystal system with *Pbnm* space group. Goldschmidt tolerance factor in ABO_3 (where A = Gd and B = Mn) compound is given by

$$t = \frac{\langle r_A \rangle + \langle r_O \rangle}{\sqrt{2}\,[\langle r_B \rangle + \langle r_O \rangle]},$$

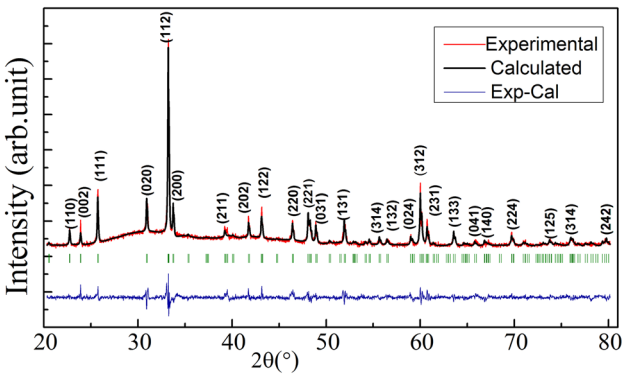

Figure 1. The powder XRD profile of GLMO manganite.

where r = ionic radius. In $GdMnO_3$ sample, when we substitute 15% Li in the place of Gd, average A and B sites radii both reduce since $r_{Li^{1+}} < r_{Gd^{3+}}$ and $r_{Mn^{4+}} < r_{Mn^{3+}}$. Tolerance factor ($t$) for GMO is 0.8518 and for GLMO is 0.8595. As the calculated value of tolerance factor (t) in Li-doped compound is higher, so we can conclude that in the doped compound, there is less distortion and better stabilization.

The room temperature optical absorption spectrum of the sample was recorded as a function of wavelength in the range of 275–800 nm (figure 2a). Absorbance is lower in the 450–800 nm range, which is an essential condition for non-linear optical applications. The optical band gap was calculated by using Tauc's formula $\alpha h\nu = A(h\nu - E_g)^n$ [15], where A is a constant, α the absorbance coefficient, E_g the band gap energy of the material and n the band gap transition dependent exponent, which depends on whether the transition is direct or indirect. Here, the value of n is 0.5, since the transition is direct one. Figure 2b shows the graph of $(\alpha h\nu)^2$ *vs.* energy ($h\nu$) of the incident photon. The linear behaviour of the curve cuts the real axis at about 3.12 eV, which is the value of optical band energy gap. To understand the magnetic behaviour and effect of monovalent substitution in the magnetic properties in GLMO, temperature-dependence magnetization was measured under $H = 50$ Oe with FC and ZFC modes. Figure 3 shows that below 50 K temperature, the sample makes a phase transition from paramagnetic to a critical state. We have plotted dM/dT *vs.* T curves in ZFC mode for $H = 50$ Oe in the inset view of figure 4. dM/dT *vs.* T plot has two minima. First minima indicate that the sample undergoes a phase transition from a paramagnetic state (PM) to an incommensurate antiferromagnetic (ICAFM) state at ∼41.32 K when $H = 50$ Oe. The second minima show that a further transition occurs from ICAFM to canted-A-type antiferromagnet (cAFM) at 20.27 K for $H = 50$ Oe. In GLMO sample, antiferromagnetic super-exchange interactions are observed in Gd^{3+}–Gd^{3+}, Mn^{3+}–Mn^{3+}, Gd^{3+}–Mn^{3+} interactions. Among them, Mn^{3+}–Mn^{3+} interaction is more significant than the other two interactions, since 3d–3d interaction is stronger than 4f–4f/3d–4f interactions. So, antiferromagnetic behaviour is observed in this sample below 42 K. Fifteen percent Li substitution transforms 30% Mn^{3+} into Mn^{4+}, which enhanced the hole density, as a result, Zener double exchange mechanism in Mn^{3+}–O–Mn^{4+} network comes into play. Owing to this weak ferromagnetism, canted-antiferromagnetic ordering is observed below 21 K. Similar transition has also been

Table 1. Structural information of GLMO manganite.

Crystal system	Space group	Cell dimensions (Å)	Volume (Å^3)	R_p (%)	R_{wp} (%)	R_{exp} (%)	GOF
Orthorhombic	*Pbnm*	$a = 5.30968$ $b = 5.77923$ $c = 7.44419$	228.4251	2.24	3.07	1.82	2.84

R_b = the profile R-factor; R_{wp} = the weighted profile R-factor; R_{exp} = expected R-factor; GOF = goodness of fit which is defined by $(R_{wp}/R_{exp})^2$.

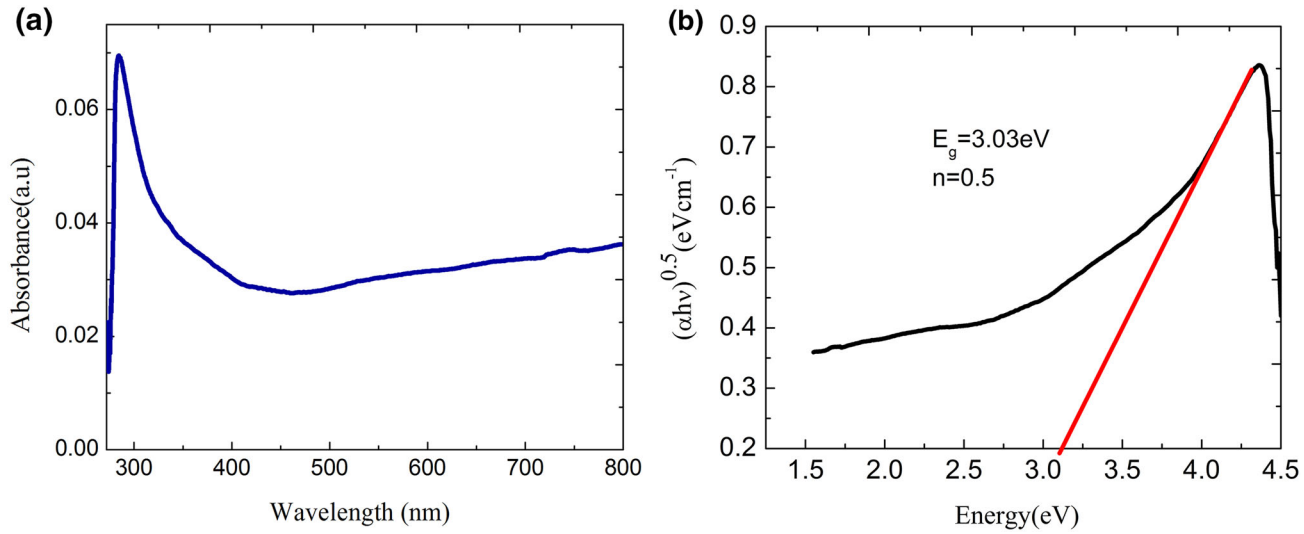

Figure 2. (**a**) Room temperature optical absorption spectrum of GLMO. (**b**) Graph of $(\alpha h\nu)^2$ *vs.* energy $(h\nu)$ of the incident photon.

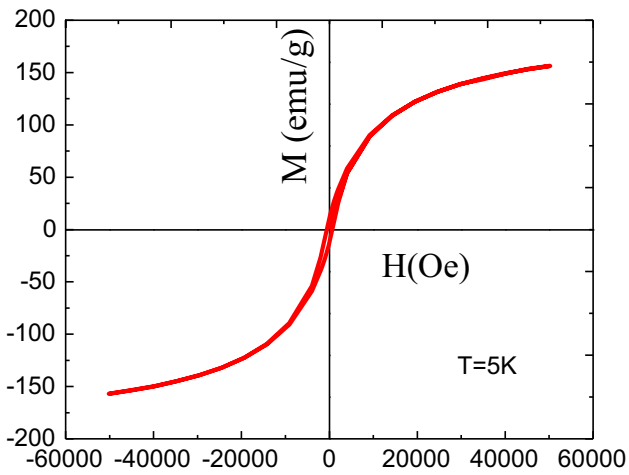

Figure 3. M–H curve at $T = 5$ K.

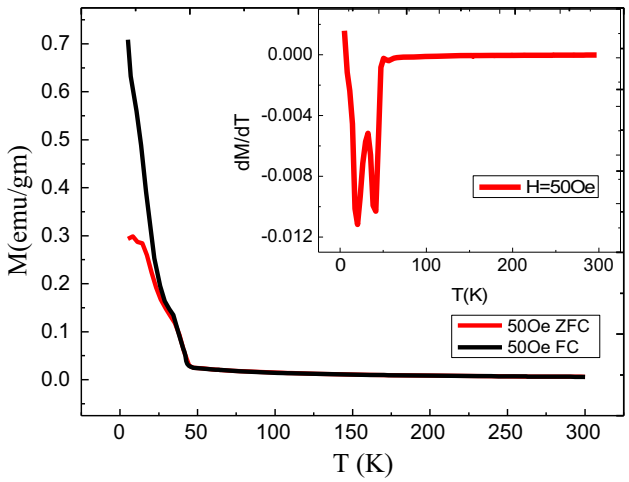

Figure 4. Temperature-dependence magnetization was measured under H is with FC and ZFC modes. Inset dM/dT *vs.* T curves in ZFC mode for $H = 50$ Oe.

observed in $GdMnO_3$ [16]. It is interesting to note that 15% doping of Li creates 30% Mn^{4+} similar to 30% doping of Ca at Gd site. However, the negative magnetization or magnetization reversal observed in $Gd_{0.7}Ca_{0.3}MnO_3$ [12,13] is absent in the present sample having same amount of Mn^{4+}.

For the better study of the magnetic field-dependent magnetization of GLMO, we have plotted M–H curve at $T = 5$ K (figure 3). Small hysteresis is present in the sample at a very low temperature (5 K) due to ferromagnetic interaction. At 5 K, the coercivity of the sample is ~655 emu g^{-1} and retentivity of the sample is ~7.41 Oe. No saturation was observed in the whole field range as expected for AFM sample [17,18]. In figure 5, inverse susceptibility *vs.* temperature graph is plotted in ZFC mode for the field values $H = 50$ Oe. We have fitted the curve with Curie–Weiss law

$$\chi = \frac{C}{[T - \Theta_{cw}]},$$

where C is the Curie–Weiss constant and Θ_{cw} the Curie–Weiss temperature. The linear fit of experimentally obtained susceptibility data intersects the $x-$axis near about -37 K, which is represented as Curie–Weiss temperature for 50 Oe field value. This negative value of Θ_{cw} indicates that there is antiferromagnetic interaction between the spins at a very low field in GLMO. Theoretical effective magnetic moment of GLMO is calculated by using the formula

$$\mu_{eff} = [0.85\mu_{eff}(Gd^{3+})^2 + 0.15\mu_{eff}(Li^{+})^2 + 0.70\mu_{eff}(Mn^{3+})^2 + 0.30\mu_{eff}(Mn^{4+})^2]^{1/2},$$

where the theoretical values of magnetic moments are taken as $\mu_{eff}(Gd^{3+}) = 7.9\mu_B$, $\mu_{eff}(Li^{+}) = 2.82\mu_B$,

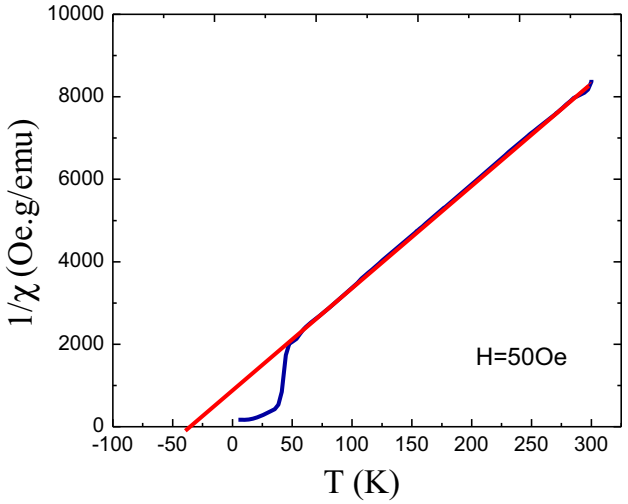

Figure 5. Inverse susceptibility *vs.* temperature graph is plotted in ZFC mode for the field values $H = 50$ Oe.

$\mu_{\text{eff}}(\text{Mn}^{3+}) = 4.9\mu_{\text{B}}$ (high spin state), $\mu_{\text{eff}}(\text{Mn}^{4+}) = 3.87\mu_{\text{B}}$. Theoretically calculated effective magnetic moment of GLMO is $\mu_{\text{eff}}^{\text{Th}} = 8.69\mu_{\text{B}}$. The experimental effective magnetic moment is determined by using the equation of Curie constant, $C = N\mu^2/3k_{\text{B}}$; where N is the Avogadro number and k_{B} the Boltzmann constant. Taking the slope $(1/C)$ of inverse susceptibility *vs.* temperature plot from the linear fit region, experimentally calculated effective magnetic moment of GLMO is determined as $8.76\mu_{\text{B}}$, which is nearly close to the theoretical value.

4. Conclusions

Impurity phase-free GLMO sample with orthorhombic *Pbmn* space group has been synthesized by using solid-state reaction route. The optical band gap of the sample estimated by using the Tauc's formula is 3.12 eV. The sample undergoes a transition from PM state to ICAFM state below T_{N} ~42 K and transforms into a cAFM state below T_{C} ~21 K. A ferromagnetic like M–H loop is observed at 5 K and no saturation in the magnetization value in the whole range of the applied magnetic field (H) indicates the presence of cAFM states. Hence, we can conclude that at 5 K, the magnetic moment of the sample is due to Gd spin ordering. The coercivity of the sample is ~655 emu g^{-1} and retentivity of the sample is ~7.41 Oe. Theoretically and experimentally calculated effective magnetic moments are well matched.

Acknowledgements

We wish to acknowledge UGC-DAE-CSR, Kolkata, for giving the instrumental facilities.

References

[1] Feyerherm R, Dudzik E, Wolter A U B, Valencia S, Prokhnenko O, Maljuk A *et al* 2009 *Phys. Rev. B* **79** 134426
[2] Pimenov A, Mukhin A A, Ivanov V Y, Travkin V D, Balbashov A M and Loidl A 2006 *Nat. Phys.* **2** 97
[3] Kimura T, Lawes G, Goto T, Tokura Y and Ramirez A P 2005 *Phys. Rev. B* **71** 224425
[4] Goto T, Kimura T, Lawes G, Ramirez A P and Tokura Y 2004 *Phys. Rev. Lett.* **92** 257201
[5] Ribeiro J L 2007 *Phys. Rev. B* **76** 144417
[6] Kimura T, Goto T, Shintani H, Ishizaka K, Arima T and Tokura Y 2003 *Nature (London)* **426** 55
[7] Cheong S W and Mostovoy M 2007 *Nat. Mater.* **6** 13
[8] Kimura T, Ishihara S, Shintani H, Arima T, Takahashi K T, Ishizaka K *et al* 2003 *Phys. Rev. B* **68** 060403
[9] Hemberger J, Lobina S, von Nidda H A K, Tristan N, Ivanov V Y, Mukhin A A *et al* 2004 *Phys. Rev. B* **70** 024414
[10] Samantaray S, Mishra D K, Pradhan S K, Mishra P, Sekhar B R, Behera D *et al* 2013 *J. Magn. Magn. Mater.* **339** 168
[11] Nandy A, Roychowdhury A, Kar T, Das D and Pradhan S K 2016 *RSC Adv.* **6** 20609
[12] Biswas S, Khan M, Pal S and Bose E 2014 *J. Supercond. Nov. Magn.* **27** 463
[13] Snyder G J, Booth C H, Bridges F, Hiskes Ron, Di Carolis Steve, Beasley M R *et al* 1997 *Phys. Rev. B* **55** 6453
[14] Biswas S, Pal S and Bose E 2014 *Indian J. Phys.* **88** 1045
[15] Singh D, Gupta R and Bamzai K K 2016 *J. Mater. Sci.: Mater. Electron.* **28** 5295
[16] Baier J, Meie D, Berggold K, Hemberger J, Balbashov A, Mydosh J A *et al* 2006 *Phys. Rev. B* **73** 100402
[17] Dutta Dimple P, Jayakumar O D, Tyagi A K, Girija K G, Pillai C G S and Sharma G 2010 *Nanoscale* **2** 1149
[18] Dutta Dimple P, Sharma G, Rajaraman A K, Yusuf S M and Dey G K 2007 *Chem. Mater.* **19** 1921